Analysis of blue and red laser performance of the infrared-pumped praseodymium-doped fluoride fiber laser

A. C. Tropper, J. N. Carter, R. D. T. Lauder, and D. C. Hanna

Department of Physics and Optoelectronics Research Centre, University of Southampton, Southampton SO9 5NH, UK

S. T. Davey and D. Szebesta

BT Laboratories, Martlesham Heath, Ipswich, Suffolk IP5 7RE, UK

Received July 27, 1993; revised manuscript received November 1, 1993

The laser performance at 491 and 635 nm of praseodymium-doped fluorozirconate fiber pumped at 1.01 μm and 835 nm is described and is interpreted with analytical solutions to the rate equations. Spectroscopic measurements of the absorption and the emission cross sections are presented, and the values are shown to be consistent with the observed lasing performance. The analytical model is shown to be a reliable indication of the optimum length of fiber for operation on the three-level 491-nm transition.

INTRODUCTION

The high-quality lanthanide-doped fluorozirconate (ZBLAN) glass fibers now available have been shown to exhibit a number of visible laser transitions,[1–9] some of which can be pumped efficiently at infrared wavelengths by means of nonlinear multistep pumping processes.[5–9] These systems appear to be increasingly promising as compact visible sources based on infrared diodes, with the merit of great simplicity, because the efficiency of the optical upconversion process does not depend on phase matching.

Pr is a unique visible laser ion offering red, green, and blue laser transitions from the same initial level.[4] A Pr-doped ZBLAN fiber pumped at two infrared wavelengths was operated at room temperature as a cw laser on transitions at 635, 605, 520, and 491 nm.[6] The upper laser level was populated in a two-step process with pump lasers at 1010 and 835 nm to excite each step resonantly. High gains were achievable on the 635-nm red transition, from which 185-mW output power was observed with an absolute optical power conversion efficiency of nearly 7%. The 491-nm blue transition terminates on thermally depopulated high-lying levels of the ground multiplet, so lasing occurs in the wing of the emission band, avoiding three-level reabsorption losses. This transition is correspondingly inefficient; nevertheless, it was the first example of a multistep infrared-pumped blue laser to operate continuously at room temperature.

To assess the ultimate potential of these lasers in optimized waveguide structures, a thorough understanding of their performance, based on reliable spectroscopically measured transition probabilities and rate-equation models that faithfully represent the optical pumping process, is essential. This paper presents a set of experimentally determined absorption cross sections, emission cross sections, and lifetimes that are sufficient to characterize visible gain in the dual-wavelength-pumped Pr-doped ZBLAN fiber laser. An elementary model is developed that relates both four-level and three-level gain to incident pump powers in an analytical form. Measurements of red and blue laser threshold for varying fiber lengths and pump conditions are shown to yield results in good agreement with this model. The essentially graphical analysis presented here is found to provide a powerful framework within which to consider the trade-offs involved in optimizing this complex system. In particular, the model is shown to provide a reliable guide to the optimum fiber length for blue lasing. Blue laser performance depends sensitively on length, and experimental investigation of this dependence involves destructively cutting back scarce and expensive fiber.

EXPERIMENTAL TECHNIQUES

Two samples of Pr-doped ZBLAN fiber were used for these experiments: fiber A had a core diameter of 4.6 μm, NA ~ 0.15, and a nominal Pr ion concentration of 560 parts in 10^6 wt., and fiber B had an elliptical core of 2.3 μm × 2.7 μm, NA ~ 0.21, and a dopant ion concentration of 1000 parts in 10^6 wt. For PrF_3 in ZBLAN glass [density 4.51×10^3 kg m^{-3} (Ref. 10)], 1 part in 10^6 wt. is equivalent to 1.37×10^{22} Pr ions m^{-3}.

A bulk-glass sample of standard ZBLAN composition doped with 5000 parts in 10^6 wt. of PrF_3 was also available. Absorption band profiles for Pr in ZBLAN glass were determined from this sample with a Perkin-Elmer UV/VIS/IR spectrophotometer, with a resolution of less than 10 wave numbers; however, absorption cross-section values at specific wavelengths were measured in fibers by excitation spectroscopy. In spectroscopic and laser experiments two argon-ion-pumped titanium sapphire lasers were used to excite the Pr ion population resonantly. A polarizing beam splitter was used to superimpose the two infrared laser beams, which could then be launched into the fiber by use of a 20× microscope objective. Launch efficiencies could not always be measured owing to our reluctance to cut back precious fiber;

0740-3224/94/050886-08$06.00

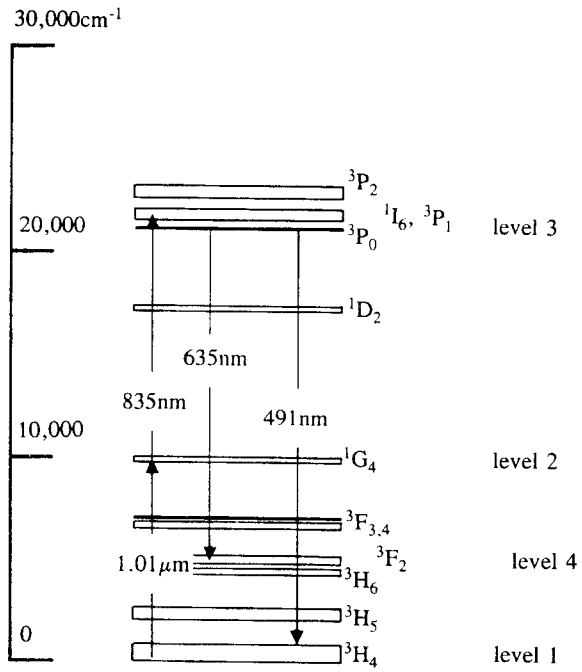

Fig. 1. Energy-level diagram for the Pr^{3+} ion showing the optical pumping cycle for infrared-pumped visible laser emission and the labeling scheme used for the rate-equation model.

however, all the experimental data were consistent with launch efficiencies of ~30% and ~20% into fibers A and B, respectively.

We made fluorescence measurements by collecting the emitted light escaping laterally from the fiber in a silica fiber bundle by means of which the light could be coupled directly to the entrance slit of a 0.25-m focal-length grating monochromator. In this sidelight geometry the absorption depth of the fiber is very small, and it can be assumed that distortion of the spectrum by reabsorption is negligible even at resonance with ground-state absorption (GSA) transitions. Visible emission was detected with a 5-cm prismatic end-window photomultiplier with an S-20 photocathode. Visible fluorescence decay curves were measured by a gated photon-counting technique. Using an acousto-optic modulator to chop the exciting laser beam and a Stanford SR400 photon counter, we found that the time resolution of this technique was 100 ns.

The fiber resonator used in the laser experiments was of the Fabry–Perot type, with feedback provided either by the Fresnel reflection at the cleaved fiber end or by a dielectric mirror optically contacted to the cleaved end, with the fiber and the mirror supported in a micromachined quartz block.

SPECTROSCOPIC MEASUREMENTS OF OPTICAL PUMPING PARAMETERS

An energy-level diagram for the trivalent Pr ion is shown in Fig. 1, in which the level-labeling scheme used here for the population rate equations is also indicated. The 1.01-μm pump beam is resonant with a GSA band and excites the Pr ion from the $^3H_4$ ground multiplet (level 1) to the $^1G_4$ multiplet (level 2), which acts as an intermediate level for the two-step pumping process. The population of this multiplet is then transferred by the excited-state absorption (ESA) of the 835-nm pump beam to a group of states with a $^1I_6 + {}^3P_1$ character that very rapidly reaches thermal equilibrium with the $^3P_0$ multiplet (level 3), which is the upper laser level. The 491-nm blue laser transition terminates on level 1, and the 635-nm red laser transition, which exhibits the highest gain, terminates on the $^3F_2$ multiplet (level 4). The physical parameters that govern this optical pumping cycle are summarized in Table 1, which shows the best value determined for each parameter from the spectroscopic measurements and the symbol used to represent each parameter in the analysis.

The GSA spectrum between 0.9 and 2.9 μm of a 13-mm-thick ZBLAN glass sample doped with 5000 parts in 10^6 wt. of Pr is shown in Fig. 2, in which each band is labeled with the multiplet on which the transition terminates. The $^3H_4 - {}^1G_4$ pump transition is evidently extremely weak compared with the others shown in this range. The peak optical density of ~0.02 shown in the figure corresponds to a cross section of $\sim 10^{-26}$ m^2 and a saturation power in fiber B of ~1.2 W. It was concluded that, provided that maximum power in the fiber core was kept an order of magnitude below this value, it was reasonable to use a laser-pumped fluorescence experiment to determine the small-signal fiber absorption coefficient and hence the absorption cross section. This was accom-

Table 1. Optical Pumping Cycle Parameters

Spectroscopic Parameter	Symbol	Value
GSA cross section, level 1 → level 2 at 1.015 μm	σ_{12}	$5.7(3) \times 10^{-26}$ m^2
ESA cross section, level 2 → level 3 at 835 nm	σ_{23}	$1.0(2) \times 10^{-24}$ m^2
Lifetime of level 2 ($^1G_4$)[a]	τ_2	110 μs
Lifetime of level 3 ($^3P_0$)	τ_3	47(1) μs
Emission cross section at 635 nm	σ_{34}	$1.8(2) \times 10^{-24}$ m^2
Emission cross section at 491 nm	σ_{31}	$0.5(1) \times 10^{-24}$ m^2
Cross section for ground-state reabsorption at 491 nm	σ_{14}	$0.02(1) \times 10^{-24}$ m^2

[a] Reference 11.

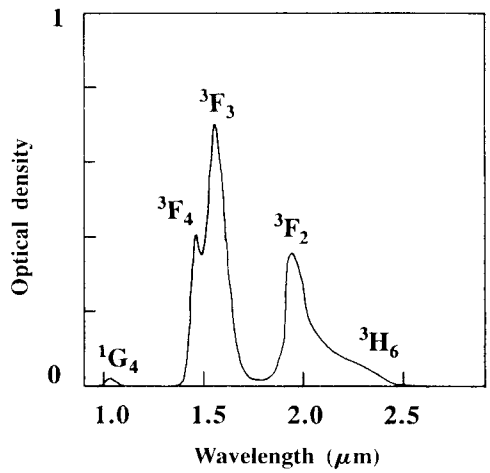

Fig. 2. Room-temperature absorption spectrum of a 13-mm-thick ZBLAN glass sample doped with 5000 parts in 10^6 wt. of Pr.

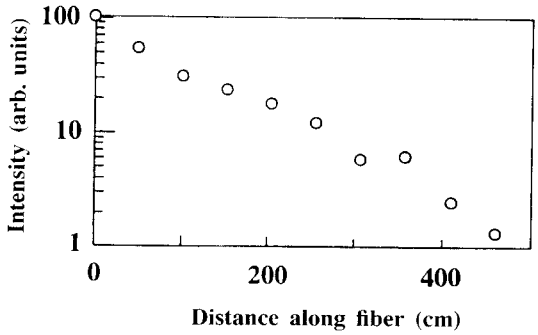

Fig. 3. Logs of intensity of 586-nm sidelight fluorescence from a length of fiber B pumped at 1.015 μm as a function of distance along the fiber.

plished in an experiment in which the fiber bundle was translated past ten turns of fiber B wound on a drum and pumped at 1.015 μm. A plot of the visible fluorescence signal versus the translation of the bundle showed a peak each time the bundle passed a turn on the drum. In Fig. 3 the logs of the peak signal values are plotted as a function of length along fiber B, deduced from the known diameter of the drum. The fluorescence signal recorded is that of the weak 586-nm emission from the $^1D_2$ level, which was found to depend linearly on pump power within experimental error over the range of power used. (The principal mechanism by which the $^1D_2$ level is excited could not be identified; because more than one photon is needed for reaching this level, one would expect a superlinear dependence on pump power at 1.015 μm. The explanation for the linear dependence observed in practice may be saturation of some ESA process.) The gradient of the curve corresponds to an absorption coefficient for fiber B of 3.9 dB m^{-1}, which is consistent, for a fiber of 1000 parts in 10^6 wt. with scattering losses at 1.015 μm of ~0.3 dB m^{-1}, with the published value of 3.4(2) dB km^{-1} parts in 10^6 wt.$^{-1}$.[10] The absorption cross section may therefore be assigned a value in the range of $5.7(3) \times 10^{-26}$ m^2.

In contrast to the weak GSA at 1.01 μm, the ESA at 835 nm is extremely strong. This property of the Pr ion enables the optical pumping at 835 nm to compete efficiently with rapid nonradiative de-excitation of the $^1G_4$ level (~10^4 s^{-1}).[11] It also leads to significant depletion of the $^1G_4$ population with only modest levels of 835-nm power in the fiber core. Studies of this effect were used to deduce a value for the ESA cross section. A 40-cm length of fiber A was pumped at one end with two infrared laser beams. The power incident upon the fiber end at each wavelength could be varied independently. The cleaved fiber end farthest from the input was passed through a 10-cm integrating sphere and was positioned in the exit port of the sphere; a power meter recorded the total transmitted pump power. In this short length of fiber only a small percentage of the power in the pump beams was absorbed, and it can therefore reasonably be assumed that the value of transmitted power at either wavelength was negligibly affected by the presence of the other beam. Because the integrating sphere contained only ~0.04 times the absorption length of the fiber at 1.01 μm, the pump power at either wavelength was effectively constant within the sphere. To determine the intracore power at either wavelength, the other beam was blocked behind the Glan–Taylor prism, and the reading on the power meter for the transmitted pump was corrected for the Fresnel reflection at the fiber end face. Pump intensities were calculated from the known fiber core dimensions, assuming a top-hat radial distribution. The variation of the visible fluorescence signal (605 nm, $^3P_0$–$^3H_6$) with 835-nm power is shown in Fig. 4, with the intracore 1.01-μm power taking the values 400, 300, and 150 mW. All three curves show a considerable degree of saturation, insofar as the greater part of the $^1G_4$ population is transferred to the $^3P_0$ level. This behavior is described by Eqs. (A1)–(A3) from the rate equation model detailed in Appendix A, from which, in the steady state, N_1 and N_2 can be eliminated to show that the $^3P_0$ population, N_3, and hence the visible emission signal should depend on the two pump intensities in the following way:

$$\frac{N_3}{N} = \left[1 + \frac{I_{23}\sigma_{23}\tau_3}{h\nu_{23}}\left(1 + \frac{h\nu_{12}}{I_{12}\sigma_{12}\tau_{12}} + \frac{I_{23}\nu_{12}\sigma_{23}\tau_3}{I_{12}\nu_{23}\sigma_{12}\tau_2}\right)\right]^{-1}. \quad (1)$$

The curves in Fig. 4 represent the best fit of Eq. (1) to the experimental points, corresponding to the value 1×10^{-24} m^2 for the fitting parameter σ_{23}. Independently determined values taken for the other parameters are those shown in Table 1. All three data sets in Fig. 4 are represented well by the calculated curves, lending support to the pump absorption cross-section values.

To verify this result, a further experiment was made in which the progressive reduction of the 1.3-μm fluorescence with increasing 835-nm pump intensity was monitored. Equation (A3) from the model predicts that in the steady state

$$N_3 = N_2 \frac{I_{23}\sigma_{23}\tau_3}{h\nu_{23}}. \quad (2)$$

Equations (1) and (2) were combined to predict the depletion of the level 2 population by ESA; the curve in Fig. 5 shows the best fit to the experimental points corresponding to a value for σ_{23} of 8×10^{-25} m^2. Compared with the visible fluorescence measurements, however, the signal-to-noise ratio was poor. Finally, it is

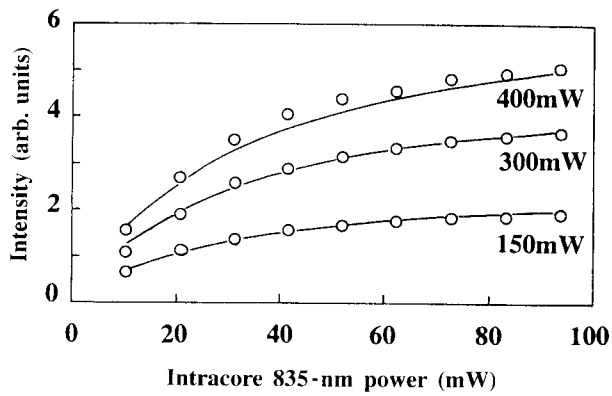

Fig. 4. Experimentally measured intensity of visible sidelight fluorescence from fiber A as a function of intracore power at 835 nm (circles) for three values of intracore power at 1.01 μm. The curves are calculated from Eq. (1) with the parameter values given in Table 1.

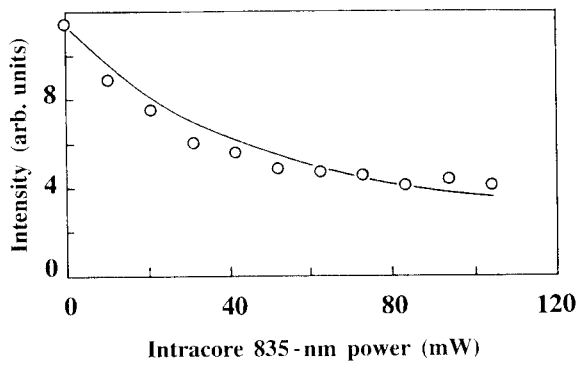

Fig. 5. Experimentally measured intensity of 1.3-μm sidelight fluorescence from fiber A as a function of intracore power at 835 nm (circles) during pumping with 500 mW of intracore power at 1.01 μm. The curve is calculated from Eqs. (1) and (2) with $\sigma_{23} = 8 \times 10^{-25}$ m^2.

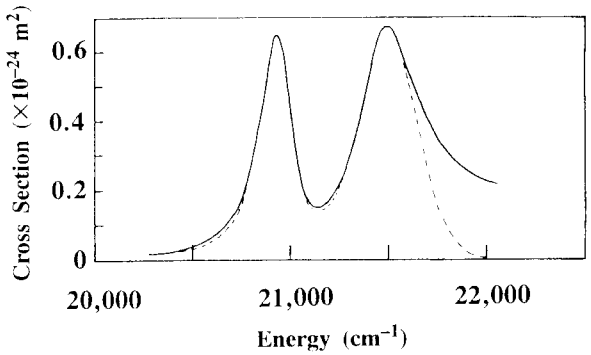

Fig. 6. Measured room-temperature absorption cross section of a Pr^{3+} ion in a ZBLAN glass host as a function of energy (solid curve) in the region of the $^3H_4 \rightarrow {}^3P_0$, $^3P_1$, $^1I_6$ absorption bands. The dashed curve represents the sum of a Lorentzian and a Gaussian band with parameters given in the text.

noteworthy that Quimby and Zheng[12] report a value of 2×10^{-24} m^2 for this cross section based on a combination of the McCumber[13] and the Judd–Ofelt analyses. These authors point out that their method may determine ESA-band profiles more reliably than absolute magnitudes, inasmuch as the Judd–Ofelt theory is known to give a poor fit for some Pr^{3+} transitions.

The magnitudes of the absorption and emission cross sections, σ_a and σ_e, at the 491-nm laser wavelength were deduced from absorption and fluorescence measurements. A spectrophotometer trace of the $^3H_4 - {}^3P_0$, $^1I_6 + {}^3P_1$ GSA band between 450 and 495 nm in the bulk ZBLAN sample is shown in Fig. 6. The data points fit closely to the sum of two lines: a Lorentzian line with a peak cross section of 0.65×10^{-24} m^2 at 478 nm, FWHM 190 cm^{-2}, containing transitions to the nondegenerate $^3P_0$ level, and a Gaussian line with a peak cross section 0.65×10^{-24} m^2 at 466 nm, FWHM 350 cm^{-1}, containing transitions to the 19 states constituting $^1I_6 + {}^3P_1$. At wavelengths shorter than ~462 nm absorption to $^3P_2$ becomes evident.

Figure 7 shows a room-temperature blue-green emission cross-section spectrum derived from a sidelight fluorescence measurement that was corrected for the detector response and that was weighted by ν^5. The peak is scaled to a value estimated with the McCumber analysis described by Miniscalco and Quimby.[14] According to this theory the emission cross-section spectrum can be derived from the absorption cross-section spectrum by the relationship[13]

$$\sigma_e(\nu) = \exp \frac{(\epsilon - h\nu)}{kT} \sigma_a(\nu), \tag{3}$$

which includes the free-energy parameter ϵ as an unknown. The underlying assumptions in this approach are, first, that the ensemble of Pr^{3+} ions is homogeneous and, second, that thermalization within a Stark-split multiplet occurs much more rapidly than any radiative process. Miniscalco and Quimby suggest an approximation in which ϵ may be estimated based on the peak energy and the overall widths of the emission and absorption bands. Following the method given in Ref. 14, we find that our spectra are consistent with 21,108 cm$^{-1} < \epsilon <$ 21,159 cm^{-1}, corresponding to a peak emission cross section of $1.8(2) \times 10^{-24}$ m^2 at 20,900 cm^{-1}. In this way absolute cross-section values are available at all energies, with an uncertainty of approximately 10%. At the blue laser transition energy the emission cross-section value is $0.5(1) \times 10^{-24}$ m^2, compared with a GSA cross-section value of $0.02(1) \times 10^{-24}$ m^2.

Despite the obvious limitations of the McCumber analysis, it was thought to provide a better emission cross-section estimate than the Fuchtbauer–Ladenburg relationship,[14] which involves integrals over the emission and absorption profiles. When applied to the emission spectrum, the Fuchtbauer–Ladenburg analysis predicted an emission cross section three times larger than that derived from the McCumber analysis, a value difficult to reconcile with the observed blue laser performance. It therefore seems likely that the transition line strength, rather than being equally shared among the nine components of the $^3H_4$ Stark levels, is markedly weighted toward the lowest-energy component.

The most reliable experimental determination of the 635-nm emission cross section was thought to be the gain measurement described in the next section, from which a value of $1.8(2) \times 10^{-24}$ m^2 was derived. This value was consistent with the observed quenching of the $^3P_0$ population by emission stimulated by a 635-nm probe beam.

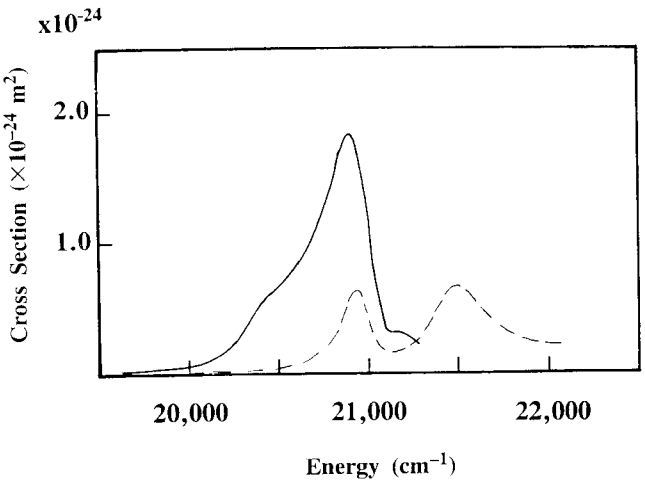

Fig. 7. Room-temperature emission cross-section spectrum of Pr^{3+} in ZBLAN glass near 21,000 cm^{-1} (solid curve). The absorption cross-section spectrum (dashed curve) is included for comparison.

In this study we used a $^1G_4$-lifetime value of 110 μs reported in the literature.[11] The dominant decay channel from this multiplet is well known to be multiphonon emission to the $^3F_4$ multiplet, mentioned in the next paragraph.

We measured the lifetime of the $^3P_0$ upper laser level by a gated photon-counting technique, using a short length of fiber B pumped at 476.5 nm directly into the $^1I_6$, $^3P_1$ states. After cutting off the pump, we observed that the fluorescence signal fell exponentially over more than five e-folds with a decay time of 47(1) μs. Thus no evidence for inhomogeneity or energy transfer appears in the decay curve. The rise of the fluorescence after we switched on the pump similarly followed a single exponential with the same characteristic time. This observation supports the idea that all the multiplets lying at lower energy than $^3P_0$ are relatively short-lived, with the exception of $^1D_2$ and $^1G_4$, which are barely populated from $^3P_0$ owing to small branching ratios and the absence of alternatives to radiative decay.

LASING THRESHOLD MEASUREMENTS

The four-level 635-nm transition was experimentally found to have such high gain that the available pump power was sufficient to achieve threshold in a resonator formed by the 4% Fresnel reflections at the bare cleaved fiber ends. This result provides the most reliable way of estimating the 635-nm emission cross section, with Eqs. (A16) and (A18), because the single-pass gain at threshold in such a resonator has a known value of 14 dB. The intracavity loss of a fiber laser is not normally known with any precision because the amount of feedback provided by a dielectric mirror butted against a fiber end face depends crucially on the flatness of the end face, the thickness of the air film, and the alignment of the two surfaces. In this experiment a 1.2-m length of fiber A was pumped with powers of 700 mW at 1.01 μm and 500 mW at 835 nm incident upon the launch objective. The fiber transmitted 250-mW power at 835 nm with the 1.01-μm pump blocked and 100-mW power at 835 nm with the 1.01-μm pump launched. The absorbed 835-nm pump power at 14-dB gain on the 635-nm transition was thus measured directly to be 150 mW, implying a value for the 635-nm emission cross section of 1.8×10^{-24} m^2.

To test the model of pump absorption, a further experiment on the 635-nm transition was set up. A low-loss resonator was assembled with two mirrors of >95% reflectivity at 635 nm. We used a 5-m length of fiber A in which >99% of the launched 1.01-μm pump was absorbed. The results are shown in Fig. 8, in which we obtained each point by setting the incident 835-nm power to a suitable value and adjusting the incident 1.01-μm power until threshold was just reached; a launch efficiency of 30% for each pump beam was assumed. The curve in Fig. 8 was calculated from Eq. (A12), in which there is one fitting parameter, the value of absorbed 835-nm pump power at threshold. This value depends experimentally on the intracavity loss, which cannot easily be measured. The best fit, shown in Fig. 8, corresponds to a single-pass intracavity loss of ~35%, which is reasonable for this resonator. The theory is in acceptably good agreement with the experimental results.

The reliability with which the model represents the blue laser performance was more difficult to test because this transition was never very far above threshold, making optimization of the launch difficult. The variation of threshold with fiber length was investigated for fibers A and B in cutback experiments, the results of which are plotted in Fig. 9. This shows the total incident infrared pump power required for reaching threshold at 491 nm in a resonator formed with two highly reflecting blue mirrors as a function of the fiber length. The incident powers at either wavelength were approximately equal at each point. After each cutting back of the fiber strenuous efforts were made to reoptimize the fiber launch and the optical contact to the mirror at the recleaved end. Nevertheless, it is unlikely that the cavity was precisely reproduced at each point; also, the background scattering loss in the fiber is to some extent lumped in discrete centers and is not exactly proportional to length. Despite these experimental difficulties a fairly well-defined optimum length was found for each fiber at which the power required for reaching threshold was at a minimum. At shorter lengths the fiber absorbs too little pump power, and at longer lengths the weakly pumped output end contributes to a net loss. The ratio of the optimum lengths for fibers A and B is approximately 2:1, consistent with the nominal dopant concentrations of 560 and 1000 parts in 10^6 wt., respectively.

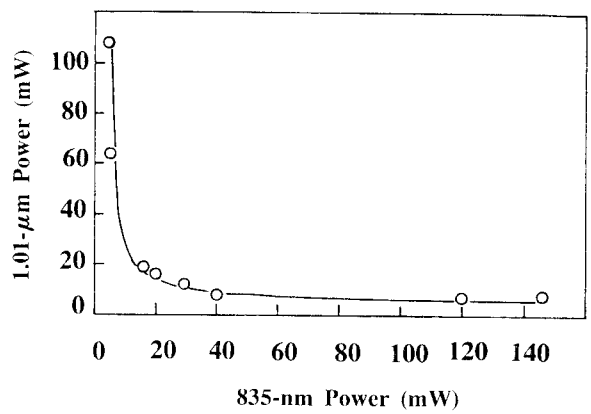

Fig. 8. Threshold power at 1.01 μm as a function of threshold power at 835 nm for lasing at 635 nm in a 10-m length of fiber A in a low-loss resonator; experimental values (circles) and theoretical curve are derived from Eq. (A12).

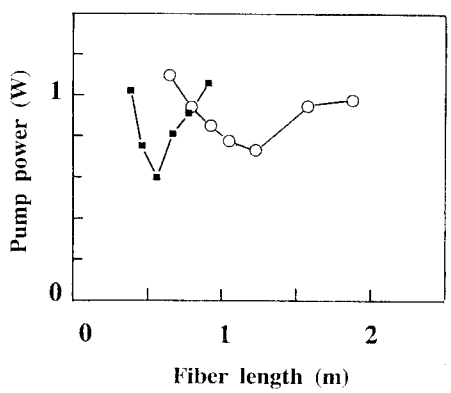

Fig. 9. Total incident infrared power at threshold for lasing at 491 nm as a function of fiber length for fiber A (circles) and fiber B (squares).

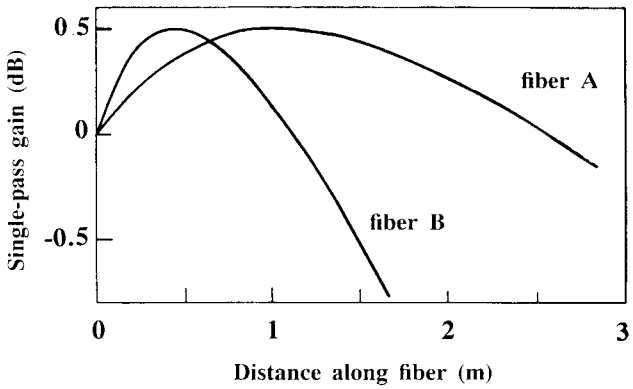

Fig. 10. Single-pass gain at 491 nm calculated from Eq. (A19) as a function of fiber length for fibers A and B.

Figure 10 shows the single-pass gain at 491 nm calculated as a function of fiber length for fibers A and B from Eq. (A19). The length dependence can be inferred from this equation because the weak 1.01-μm absorption is unsaturated, and this pump field can be assumed to have a Beer's-law dependence with the small-signal absorption coefficient. To generate these curves we adjusted the pump powers, which were assumed to be the same at the two wavelengths, until the maximum in the single-pass gain came to 0.5 dB, a value believed to be typical of the best high-Q cavities achievable by the techniques described here. The calculated optimum lengths were found to be fairly insensitive to the maximum gain, so this approach reduced reliance on launch efficiency estimates. For fiber B the calculated curve corresponds to a launched power of 200 mW, ~95 mW of which is absorbed. The calculated curves shown in Fig. 10 predict optimum fiber lengths of ~1 and ~0.5 m for fibers A and B, respectively, in good agreement with the experimental results presented in Fig. 9.

DISCUSSION

The research described here shows that a simple rate equation is adequate to describe three- and four-level gain in a Pr-doped ZBLAN fiber laser pumped at GSA and ESA bands by two infrared wavelengths. The lifetimes and the cross sections that control the optical pumping cycle were spectroscopically determined in a straightforward way to within 10–20%.

The features of the Pr:ZBLAN upconversion laser that permit such a simple quantitative analysis, the dual-wavelength-pumping scheme and the high first-step saturation intensity, are of course precisely those that impose severe limitations on its efficiency and practicality. In this regard Pr compares unfavorably with Tm, which is the only other lanthanide ion for which a blue upconversion laser transition has been demonstrated in fluoride fiber.[9] Nevertheless, all lasers of this type suffer from inherent limitations: the blue and the green transitions will tend to be three level or self-terminating, the choice of intermediate level is limited and usually involves inconvenient pump wavelengths, and the typically rather small transition cross sections will require pump intensities of the order of 1 GW m^{-2} at threshold. In today's upconversion fiber lasers these limitations are offset by the advantages of the waveguide geometry; therefore, in the future, fibers with higher numerical aperture and correspondingly better optical confinement may demonstrate significantly lower threshold and enhanced overall conversion efficiency. Improved power conversion efficiency on the low-gain blue transition would also result from improvements in fiber-fabrication technology, permitting reduction of scattering losses at the lasing wavelength, which currently are typically ~0.6 dB m^{-1}.

The most important application of this model is perhaps the analytical determination of the length of the fiber, which minimizes threshold on the three-level blue transition. Our results suggest that this approach might be fruitfully applied to the more complex problem of determining the fiber length at which the blue output power is maximum for a given combination of pump power, output coupling, and fiber design.

Blue solid-state lasers are particularly vulnerable to optical damage because the laser photon energy represents a significant fraction of the band gap. ZBLAN fiber has not yet been well characterized in this respect; nevertheless, we do not observe a tendency for the blue or the green laser threshold to increase with operating time over periods of the order of an hour. Finally, it is interesting that the energy of a 491-nm photon is sufficient to populate states in the tail of the fluoride glass conduction band by absorption from the $^3P_0$ state. If significant ESA involving energy transfer to the matrix were present, this might be expected to reduce the 491-nm gain significantly. The modeling suggests that no such effect occurs, and the low gains experimentally observed are consistent with an isolated Pr ion. This is an encouraging conclusion for short-wavelength fluoride fiber lasers generally.

APPENDIX A. RATE-EQUATION MODEL

The gain of the upconversion laser can be analyzed with elementary rate equations describing the populations N_2 and N_3 of levels 2 and 3, respectively. Both pump-laser modes are assumed to have uniform intensities, I_{12} (1.01 μm) and I_{23} (835 nm), over the fiber core, and a top-hat profile is similarly assumed for the dopant distribution; this approximation is made with the recognition that the fiber is multimode at both the 491- and the 635-nm emission wavelengths and that filling factors are likely to represent an error in the model that is small compared with uncertainties in the spectroscopically determined transition probabilities.

In constructing the rate equations, thermalization of the $^1I_6 + ^3P_1$ and $^3P_0$ populations is assumed to be instantaneous on the optical pumping time scale, and stimulated emission at the 835-nm pump wavelength from thermally depopulated levels is therefore neglected, although stimulated emission at the 1.01-μm pump wavelength is taken into account.

Experimentally it was found that excitation into the ^3P multiplets yielded extremely small quantities of $^1D_2$ emission, suggesting both that the radiative branching ratio to this level is tiny and that multiphoton emission across this ~3800-cm^{-1} gap is as negligible, as one would expect in a glass matrix with a vibrational spectrum that cuts off beyond 600 cm^{-1}. The model therefore contains the assumption that at any instant only levels 1–3 are sig-

nificantly occupied and that there are no other reservoirs for population:

$$N = N_1 + N_2 + N_3 . \tag{A1}$$

The rate equation for N_2 takes the form

$$\frac{dN_2}{dt} = \frac{I_{12}}{h\nu_{12}}(N_1\sigma_{12} - N_2\sigma_{21}) - \frac{I_{23}}{h\nu_{23}}N_2\sigma_{23} - \frac{N_2}{\tau_2}, \tag{A2}$$

simplified by the omission of a feeding term from level 3, which will in practice be small. The rate equation for N_3 takes the form

$$\frac{dN_3}{dt} = \frac{I_{23}}{h\nu_{23}}N_2\sigma_{23} - \frac{N_3}{\tau_3}, \tag{A3}$$

where, because the aim of the modeling is to establish upper limits on the achievable unsaturated gain, only spontaneous-radiative-decay processes are included.

The principal difficulty in modeling this two-step pumping scheme is that the evolution of one pump field along the fiber is interdependent with that of the other. The decay of intensity in each pump beam along the fiber is therefore governed by a pair of coupled differential equations to which closed-form solutions cannot be obtained. However, the variation of intensity in the 1.01-μm pump beam, I_{12}, can readily be evaluated as a function of the 835-nm pump intensity I_{23}, whence some useful results on the gain of the dual-pumped system can be derived.

The equations describing the dependence of I_{12} and I_{23} on z, the distance traveled along the fiber, are

$$\frac{dI_{12}}{I_{12}} = (N_2\sigma_{21} - N_1\sigma_{12})dz , \tag{A4}$$

$$\frac{dI_{23}}{I_{23}} = -N_2\sigma_{23}dz . \tag{A5}$$

Dividing Eq. (A4) by Eq. (A5), we obtain

$$\frac{dI_{12}I_{23}}{dI_{23}I_{12}} = \frac{N_1\sigma_{12} - N_2\sigma_{21}}{N_2\sigma_{23}} . \tag{A6}$$

From Eq. (A2) we find that in a steady state N_2 and N_1 must be related by

$$N_1 = N_2\left(\frac{h\nu_{12}}{\sigma_{12}\tau_2 I_{12}} + \frac{\sigma_{23}\nu_{12}I_{23}}{\sigma_{12}\nu_{23}I_{12}} + \frac{\sigma_{21}}{\sigma_{12}}\right). \tag{A7}$$

Substituting N_1/N_2 from Eq. (A7) into Eq. (A6) gives

$$dI_{12} = dI_{23}\left(\frac{h\nu_{12}}{\tau_2\sigma_{23}I_{23}} + \frac{\nu_{12}}{\nu_{23}}\right), \tag{A8}$$

which can be integrated as follows:

$$i_{12} = \ln(i_{23}) + \eta i_{23} + K , \tag{A9}$$

where

$$i_{12} = \frac{I_{12}}{I_0}, \qquad i_{23} = \frac{I_{23}}{I_0}, \tag{A10}$$

$$I_0 = \frac{h\nu_{12}}{\tau_2\sigma_{23}}, \qquad \eta = \frac{\nu_{12}}{\nu_{23}} . \tag{A11}$$

The application of limits to Eq. (A9) eliminates the integration constant:

$$\Delta i_{12} = \ln\left[\frac{i_{23}(0)}{i_{23}(0) - \Delta i_{23}}\right] + \eta\Delta i_{23} , \tag{A12}$$

where

$$\Delta i_{jk} = i_{jk}(0) - i_{jk}(L) \tag{A13}$$

and the coordinates 0, L refer to the input and the output ends of the fiber, respectively.

In Fig. 11 the normalized intracore 1.01-μm intensity i_{12} is plotted as a function of the normalized intracore 835-nm intensity i_{23} according to Eq. (A9). This is a universal curve that has the same shape for all combinations of incident intensities and for all Pr-doped fibers irrespective of their dopant concentration, core radius, and numerical aperture. The origin on the horizontal axis is fixed, and the origin on the vertical axis can slide up and down, depending on the value of the integration constant K, which must be set to give the correct initial combination of i_{12} and i_{23} corresponding to the actual launched values of 1.01-μm and 835-nm power at the input end of the fiber. The normalization intensity I_0, defined by Eqs. (A11), corresponds to a boundary between the saturated and the unsaturated pumping regimes; for $i_{23} \gg 1$ the curve tends to a straight line with gradient η, and for $i_{23} \ll 1$ the curve becomes logarithmic and has the

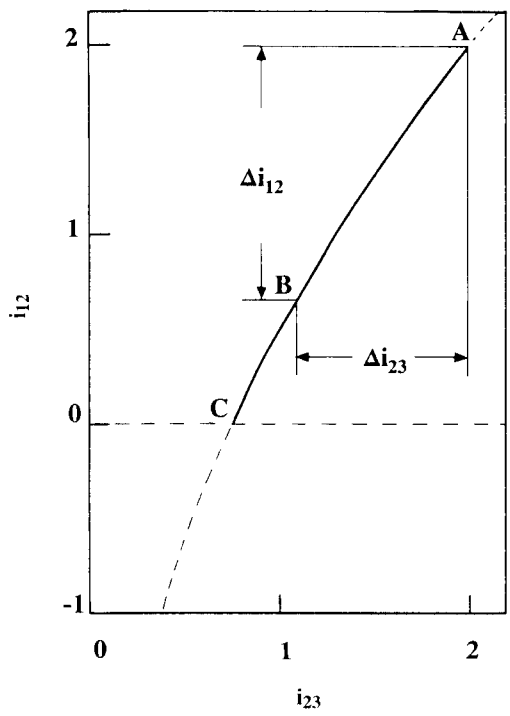

Fig. 11. Plot of Eq. (A9) relating the normalized pump intensity at 1.01 μm, i_{12}, in the fiber core to the normalized pump intensity at 835 nm, i_{23}. The origin of the i_{12} axis is set to give the hypothetical pump condition $i_{12} = i_{23} = 2$ at point A corresponding to the input end of a fiber. At some position farther down the fiber corresponding to point B the changes in pump intensity, Δi_{12} and Δi_{23}, can be read from the curve. Point C, where the curve crosses the axis, corresponds to an infinite length of fiber and defines the maximum fraction of the 835-nm pump that will be absorbed, given the values for the pump intensities at the input end.

Table 2. Saturation Intensities and Powers

Intensity ($W\ m^{-2}$)	Power: Fiber A ($A_{co} = 1.66 \times 10^{-11}\ m^2$)	Power: Fiber B ($A_{co} = 4.88 \times 10^{-12}\ m^2$)
I_0, 1.8×10^9	$A_{co}I_0$, 30 mW	$A_{co}I_0$, 9 mW
$h\nu/\sigma_{34}\tau_3$, 2.8×10^9	W_{34}, 47 mW	W_{34}, 13 mW
$h\nu_{23}/\sigma_{31}\tau_3$, 1.0×10^{10}	W_{31}, 168 mW	W_{31}, 49 mW

vertical axis as an asymptote. The curve thus provides a convenient graphical device for investigating the efficiency of the dual-wavelength-pumping process under a range of initial conditions. Note that Eq. (A9) remains valid regardless of whether the fiber is above threshold on any transition, inasmuch as Eq. (A3), in which stimulated emission processes were neglected, is not needed for its derivation.

From the values given for τ_2 and σ_{23} in Table 1 we obtain an estimate for the normalization intensity I_0 of $1.8 \times 10^9\ W\ m^{-2}$, which corresponds to a power P_0 of 30 mW in fiber A and 9 mW in fiber B.

The exponential gain coefficient for the red transition, Γ_{34}, is given by an integral along the length of the fiber from the input end, $z = 0$, to the output end at $z = L$:

$$\Gamma_{34} = \int_0^L N_3\sigma_{34}\mathrm{d}z\,. \tag{A14}$$

From the steady-state solution of Eq. (A3) and from Eq. (A5) we obtain

$$\Gamma_{34} = \int_0^L \frac{N_2 I_{23}}{h\nu_{23}/\sigma_{23}\tau_3}\,\sigma_{34}\mathrm{d}z = \int_L^0 \frac{\mathrm{d}I_{23}}{h\nu_{23}/\sigma_{34}\tau_3}\,. \tag{A15}$$

Thus the gain coefficient is given by

$$\Gamma_{34} = \frac{\Delta P_{23}}{W_{34}}\,, \tag{A16}$$

where ΔP_{23} is the absorbed power at 835 nm:

$$\Delta P_{23} = A_{co}[I_{23}(0) - I_{23}(L)] \tag{A17}$$

and W_{34} is a power characteristic of the transition given by

$$W_{34} = A_{co}h\nu_{23}/\sigma_{34}\tau_3\,, \tag{A18}$$

with A_{co} being the fiber core area.

The net gain at 491 nm, reduced by ground-state reabsorption, has the exponential coefficient

$$\Gamma_{31} = \int_0^L N_3\sigma_{31}\mathrm{d}z - \int_0^L N_1\sigma_{13}\mathrm{d}z\,. \tag{A19}$$

The first term in this expression is proportional to the absorbed power at 835 nm according to the argument given for Γ_{34} above. The second term is in practice indistinguishable from the small-signal absorption because σ_{12} is so small that the first pump step is not saturated under experimentally realizable pump intensities; thus

$$\Gamma_{31} = \frac{\Delta P_{23}}{W_{31}} - N\sigma_{13}L\,, \tag{A20}$$

where

$$W_{31} = A_{co}h\nu_{23}/\sigma_{31}\tau_3\,. \tag{A21}$$

The key results of this elementary model are the pump intensity interdependence, Eqs. (A9) and (A12), and the exponential gain coefficient expressions, Eqs. (A16) and (A20). These equations involve constants with dimensions of intensity for which estimates based on the cross sections and the lifetimes are tabulated in Table 2, together with the corresponding power values for the two fibers studied here.

ACKNOWLEDGMENTS

This research was supported by the Science and Engineering Research Council (SERC). J. Carter and R. Lauder receive Cooperative Awards in Science and Engineering studentships funded by SERC and BT Laboratories.

REFERENCES

1. J. Y. Allain, M. Monerie, and H. Poignant, Electron. Lett. **26,** 166–168 (1990).
2. J. Y. Allain, M. Monerie, and H. Poignant, Electron. Lett. **26,** 261–263 (1990).
3. J. Y. Allain, M. Monerie, and H. Poignant, Electron. Lett. **27,** 189–191 (1991).
4. R. G. Smart, J. N. Carter, A. C. Tropper, D. C. Hanna, S. F. Carter, and D. Szebesta, Opt. Commun. **86,** 333–340 (1991).
5. J. Y. Allain, M. Monerie, and H. Poignant, Electron. Lett. **27,** 1156–1157 (1991).
6. R. G. Smart, A. C. Tropper, D. C. Hanna, S. T. Davey, S. F. Carter, and D. Szebesta, Electron. Lett. **27,** 1307–1308 (1991).
7. T. J. Whitley, C. A. Millar, R. Wyatt, M. C. Brierley, and D. Szebesta, Electron. Lett. **27,** 1785–1786 (1991).
8. J. Y. Allain, M. Monerie, and H. Poignant, Electron. Lett. **28,** 111–113 (1992).
9. S. G. Grubb, K. W. Bennett, R. S. Cannon, and W. F. Humer, Electron. Lett. **28,** 1243–1244 (1992).
10. P. W. France, ed., *Fluoride Glass Optical Fibres* (Blackie, London, 1990).
11. Y. Ohishi, T. Kanamori, T. Kitagawa, S. Takahashi, E. Snitzer, and G. H. Sigel, Opt. Lett. **16,** 1747–1749 (1991).
12. R. S. Quimby and B. Zheng, Appl. Phys. Lett. **60,** 1055–1057 (1992).
13. D. E. McCumber, Phys. Rev. A **134,** A299–A306 (1964).
14. W. J. Miniscalco and R. S. Quimby, Opt. Lett. **16,** 258–260 (1991).
15. J. L. Adam and W. A. Sibley, J. Non-Cryst. Solids **76,** 267–279 (1985).